PROGRESS IN PHOTOVOLTAICS: RESEARCH AND APPLICATIONS
Prog. Photovolt: Res. Appl. (2011)
Published online in Wiley Online Library (wileyonlinelibrary.com). DOI: 10.1002/pip.1133

RESEARCH ARTICLE

A validated SPICE network simulation study on improving tunnel diodes by introducing lateral conduction layers

Marc Steiner*, Wolfgang Guter, Gerhard Peharz, Simon P. Philipps, Frank Dimroth and Andreas W. Bett

Fraunhofer Institute for Solar Energy Systems ISE, Heidenhofstr. 2, 79110 Freiburg, Germany

ABSTRACT

In this work, network simulations using LTSpice (Linear Technology, Milpitas, CA, USA) for monolithic triple-junction solar cells have been performed. In order to simulate the internal structure correctly, the integration of the tunnel diode into the network simulation was mandatory. The tunnel-diode characteristics are modeled by LTSpice's arbitrary behavioral current sources. The integration of tunnel-diode characteristics into the network model was validated by comparison of simulated and experimental data. Lattice-matched triple-junction solar cells were examined under homogenous illumination between 1 and 1900 suns as well as under non-uniform digital irradiance. The verified model was then used to study the influence of lateral current spreading in layers surrounding the tunnel diodes. It is shown that a lateral current spreading from high to low illumination intensity regions cannot prevent the tunnel diode from switching to thermal diffusion under the used Gaussian illumination profile as it appears in concentrator photovoltaic applications. Furthermore, resistance regimes of the lateral conducting layers were identified, which would enable a current spreading that is high enough to transport all current exclusively by tunneling. It is shown that the presence of at least one additional layer above and one below the tunnel diode is mandatory. Finally, the necessary layer thicknesses using $Al_{x-1}Ga_xAs$ as lateral conducting layers are calculated for different doping concentrations and mole fractions x. Copyright © 2011 John Wiley & Sons, Ltd.

KEYWORDS

simulation; triple-junction solar cells; concentrator cells; tunnel diode; lateral conduction layers; SPICE

***Correspondence**

Marc Steiner, Fraunhofer Institute for Solar Energy Systems, Heidenhofstr. 2, 79110 Freiburg, Germany.
E-mail: marc.steiner@ise.fraunhofer.de
Now with AZUR SPACE Solar Power GmbH.

Received 21 December 2010; Revised 17 March 2011

1. INTRODUCTION

Currently, the highest efficiency for any solar cell is achieved with monolithically stacked III–V triple-junction solar cells [1]. The electrical interconnection of the three subcells is realized by highly doped, optically transparent layers forming a tunnel junction [2]. In concentrator solar cells, current densities of up to 40 A/cm^2 have to be transmitted by these tunnel diodes, preferably with a low drop in voltage. Beneath a peak current density called J_{Peak}, the tunnel diode allows a low resistive tunnel transport between two subcells. However, current densities higher than J_{Peak} are transmitted by high resistive thermal diffusion, which strongly reduces the power output of the solar cell. In concentrator photovoltaic applications, solar cells are often illuminated by an inhomogeneous illumination profile. With this profile, low-intensity regions below J_{Peak} and high-intensity regions above J_{Peak} appear in solar cells. The influence of an illumination profile in combination with a specific tunnel-diode characteristic on the *I–V* curve of a triple-junction solar cell is investigated in this work.

Many models simulating the electrical behavior of solar cells or the characteristics of tunnel diodes have already been developed. A well-known method to simulate the electrical properties of solar cells is to divide the cell into smaller subcircuits representing different parts of the solar cell and model every subcircuit by an electrical circuit as described by the two-diode model. Circuit simulators like SPICE [3] are commonly used to calculate the *I–V*

characteristic. These network simulations have been used for many different applications, like front contact grid optimization [4], examining dark *I–V* curves [5], or studies of non-uniform light profiles on solar cells [6,7]. However, these investigations neglect the influence of tunnel diodes. Another common approach is to use semiconductor simulation environments to model III–V multi-junction photovoltaic devices including tunnel diodes [8–11]. However, these approaches do not calculate the *I–V* characteristic of solar cells under inhomogeneous illumination that occurs in concentrator photovoltaics. Therefore, in this work, a method to implement tunnel-diode characteristics into a network simulation environment has been established and verified. It should be noted that, recently, Espinet [12] used a similar approach.

The integration of tunnel-diode characteristics into the network simulation environment makes it possible to examine the behavior of multi-junction solar cells under inhomogeneous illumination and to capture the transition from low resistive tunneling to high resistive thermal diffusion transport. In this work, the measured electrical characteristics of a tunnel diode are integrated into a network model. Tunnel-diode characteristics are implemented in the network simulation through LTSpice's arbitrary behavioral current sources. Practically, this was carried out in an iterative manner: one simulated and one measured *I–V* curve are compared while adjusting the *I–V* characteristic of the voltage-dependent current source in LTSpice. The iteration stopped when the simulated and measured *I–V* curve is aligned. This approach makes it possible to adapt the behavior of a specific real tunnel diode within a solar cell from one *I–V* curve at a distinct concentration. As will be shown later, with this approach, *I–V* curves of triple-junction solar cells measured under uniform illumination between 1 and 1900 suns (1 sun corresponds to 1000 W/m^2) can be calculated. The validation showed an excellent agreement between simulation and measured data. Furthermore, the ability of the developed model to calculate the *I–V* characteristic of triple-junction solar cells under varying non-uniform digital illumination was experimentally verified.

As an application of the developed network simulation environment, a Gaussian illumination profile as it occurs in concentrator photovoltaic systems was applied to a lattice-matched triple-junction solar cell. Thereby, it has been demonstrated that the lateral current spreading is not enough to prevent the tunnel diode from operating in the thermal diffusion transport mode. Braun *et al.* demonstrated in [13] experimental evidence of a prominent dependence of the tunnel-diode transition on the degree of localized irradiation in multi-junction cells. This effect was explained by the suggestion of a lateral current spreading. The results shown in this paper agrees with the lateral current spreading suggested by Braun *et al.* [13]. It is presented that the implementation of two additional lateral conduction layers around the tunnel diode is necessary to increase the lateral current spreading sufficiently. As a realization of those results, the minimum thicknesses of $Al_{x-1}Ga_xAs$ lateral conducting layers were calculated for different doping concentrations and composition factors x.

2. MODEL DESCRIPTION

2.1. Modeling approach

A solar cell based on semiconducting layers is often described by the two-diode model. The two-diode model describes the solar cell through an electrical circuit consisting of resistances, diodes, and current sources. The main drawback of this model is the missing spatial distribution, which is why an inhomogeneous illumination of the solar cell or the distribution of the series resistances [14] cannot be modeled accurately. A common strategy, also used in this work, to expand the two-diode model with a spatial distribution is to divide a solar cell into small elementary cells. Galiana *et al.* [15] and Nishioka *et al.* [6], for instance, used related modeling approaches. The novel aspect of the developed model here is the implementation of tunnel-diode effects in network simulations and its verification with measured data.

The network model used in this work is based upon the model already described in detail by Steiner *et al.* [4]. In the following sentences, this network model will be briefly introduced and the modifications explained in detail. The two elementary cells used in the network circuit model are shown in Figure 1. They consist of three elementary subcells (top, middle, and bottom). Each subcell is modeled by an electrical circuit based on the two-diode model. The subcells are connected in series by voltage-dependent current sources, thus modeling the tunnel-diode effect. The implementation of tunnel diodes into the network model is described in more detail in Section 2.3. The difference between the two elementary cells is that one describes the dark area under the contact grid, whereas the other contains in addition ideal current sources modeling the area where photocurrents are generated. All of them have series resistances to model the lateral conducting layers (LCL) and two diodes describing the saturation currents of the p–n junction. These two diodes represent the losses by recombination in the neutral (J_{01}) and in the depletion region (J_{02}). One ideal current source represents the light-generated current and completes each of the three illuminated elementary subcells. The contact grid is modeled by ohmic resistances, one representing the metal–semiconductor contact (r_C) and one the resistance of the grid line (r_F). A distinct area ($A(x,y)$) depending on the type and the position (x,y) of the elementary cell is assigned to all electrical elements.

Figure 2 shows the complete solar cell model based on interconnected elementary cells. The elementary cells are connected in parallel by the lateral conducting series resistances. The resulting network was solved numerically by the circuit simulator SPICE. In this work, LTSpice from Linear Technology Corporation [16] was used. A circuit simulator can calculate the current running through

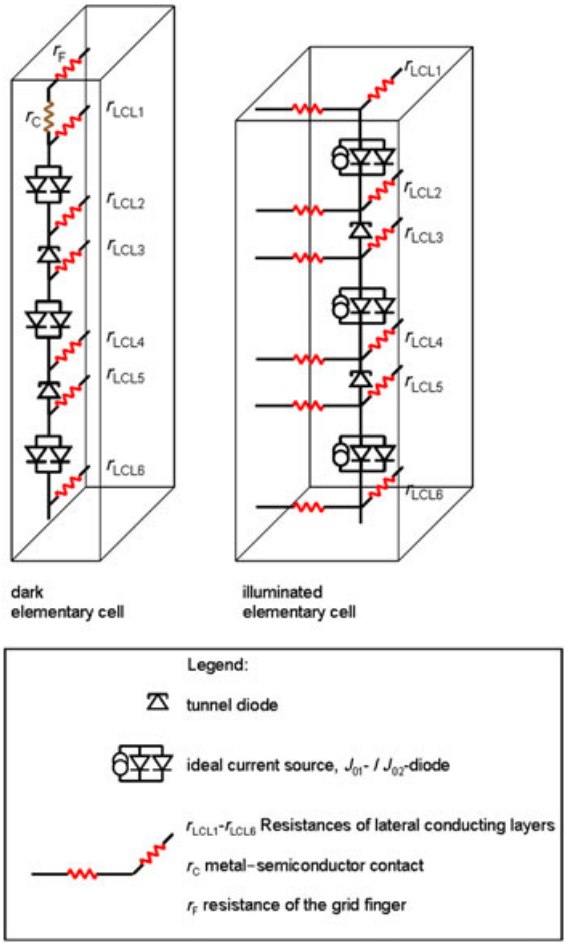

Figure 1. The two types of elementary cells used to simulate the complete solar cell. The sub-cells are simulated with the two-diode model. The dark elementary cell models parts of the solar cell that are shaded by the contact grid, and the illuminated elementary cell substitutes the area of the solar cell where the photocurrent is generated (LCL, lateral conduction layer).

each electrical component placed between two nodes and the voltages at each node in the network [3]. An accurate calculation of a solar cell's *I–V* curve can be obtained when the simulation results do not change significantly with increases in the number of elementary cells. Note that ohmic shunts described by a parallel resistance in the two-diode model are neglected. The shunts of the examined solar cells have a negligible influence under the applied illumination intensities. A reduction of network elements shortens the calculation duration. Therefore, the shunts are omitted.

2.2. Parameter identification

Every solar cell has its own characteristic, depending on the internal semiconductor structure and the technological processing applied. Therefore, the successful application of the developed model requires detailed knowledge of the investigated triple-junction solar cell. The layer structure of this solar cell is illustrated in Figure 3. The solar cell consists of a gallium–indium–phosphide top cell ($Ga_{0.50}In_{0.50}P$), a gallium–indium–arsenide middle cell ($Ga_{0.99}In_{0.01}As$), and a germanium bottom cell (Ge). The top and the middle subcells are connected by the top tunnel diode, which is comprised of GaInP and AlGaAs. The middle and the bottom subcells are connected by the bottom tunnel diode, which consists of GaInAs and AlGaInAs. The simulation of the solar cells requires input parameters. These input parameters can be divided into different categories: ohmic resistivities, photogenerated currents and saturation currents for each subcell. The input parameters used are summarized in Table I. They were derived by different experimental methods annotated in the following paragraphs. The tunnel diodes are considered by the *J–V* characteristic shown in Figure 5.

The light-generated current density $J_L(C = 1, 1000\,W/m^2)$, which corresponds to the current-limiting top cell J_{SCtop}, was measured with a calibrated three-source sun simulator. The J_{SCmid} of the middle cell cannot be measured directly as it was carried out for the top cell. Therefore, the J_{SCmid} of the middle cell is obtained from the spectrometric characterization [17]. The great excess current of the bottom cell results in a lower sensitivity of the solar cell characteristic on that parameter. Therefore, the accuracy of a spectrometric characterization is not necessary. The J_{SCbot} of the germanium bottom cell is calculated with its measured external quantum efficiency and by assuming the AM1.5d spectrum. The dark currents in the neutral (J_{01}) and in the depletion zone (J_{02}) of each subcell are derived from component cells. Component cells are cells with the same internal structure but with only one subcell electrically active. The saturation currents of the middle cell were extracted from suns-V_{OC} measurements [18] by fitting the two-diode equation. The available top component cell does not permit measurement at high concentration, which is mandatory for the suns-V_{OC} method. Therefore, the values for the top cell are derived from dark *I–V* measurements. For the bottom Ge cell, no component cell was available. Thus, the saturation currents of the bottom cell were obtained by fitting the simulated data to the measured $V_{OC}(C)$ curve of the triple-junction solar cell.

Two of the unknown resistivities were derived by the transmission line model [19]: the metal–semiconductor contact resistivity (ρ_C) of the front contact and of the rear contact (ρ_{RC}). The resistivity of the metallization (ρ_M) was determined by measuring the voltage drop in a single grid line and by applying Ohm's law. The sheet resistances of the lateral conducting layers cannot be easily measured within a triple-junction solar cell and were calculated using the equation $r_{Sheet} = (d \cdot \mu \cdot n \cdot e)^{-1}$, in which d is the thickness of the layer, μ is the mobility, n is the doping concentration, and e is the elementary charge. The mobilities were calculated based on the empirical model developed by Sotoodeh *et al.* [20]. The electrically active doping concentration n is the concentration measured via electrochemical capacity-voltage profiling (ECV). Figure 3 shows the resistivities of the lateral conduction layers, which are assumed to be connected in parallel.

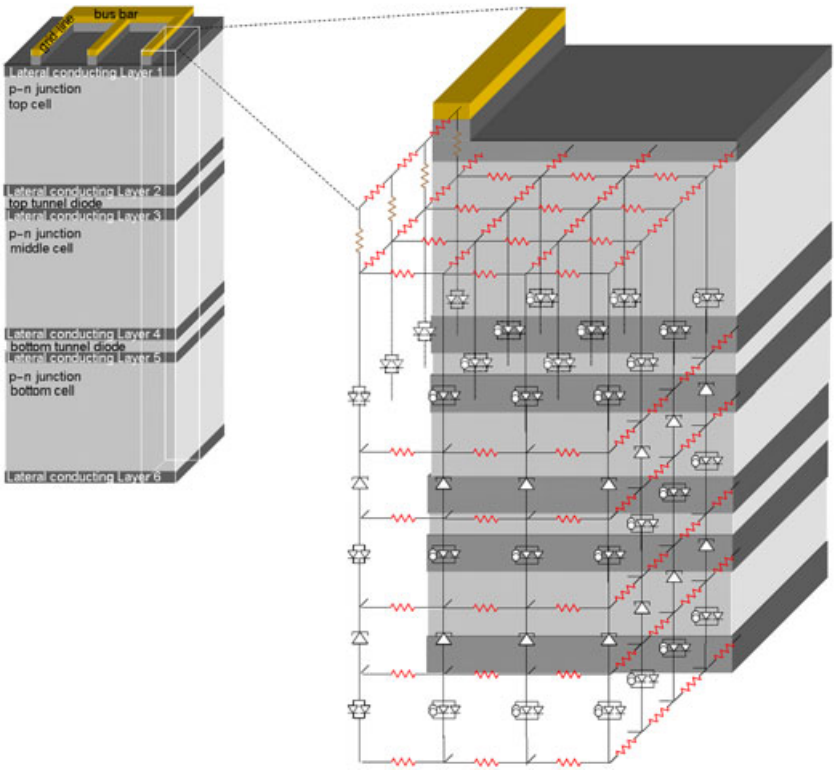

Figure 2. Distributed network model of a triple-junction solar cell consisting of two types of elementary cells based on the two-diode model. The model includes the complete solar cell including bus bars, grid lines, and saturation as well as photocurrents and tunnel diodes.

2.3. Implementation of the tunnel diodes into the network model

In the developed network model, tunnel junction effects are included using LTSpice's arbitrary behavioral current sources, the behavior of which can be predefined as a correlation of current density to voltage drop. Ideally, the measured *J–V* characteristic of the real tunnel diode inside the triple-junction solar cell should be used for the arbitrary current sources. However, the *J–V* characteristic of a tunnel diode inside a triple-junction solar cell cannot be measured directly. In addition, it is not possible to identify whether the top or the bottom tunnel diode has the lower J_{Peak}. In this work, the first problem is solved by extracting the *J–V* characteristic for parameterization of the arbitrary current sources out of a measured *I–V* curve of a lattice-matched triple-junction solar cell. The triple-junction cell was measured at 847 suns, and the *I–V* curve, which clearly shows the influence of the tunnel-diode characteristic, is displayed in Figure 4. For comparison, the calculated *I–V* curve of that solar cell without tunnel-diode effects is also indicated in Figure 4. The *J–V* characteristic used for the arbitrary current source in LTSpice is now adjusted iteratively until the calculated *I–V* curve matches the measured one. The resulting correlation of current density and voltage drop of the simulated tunnel diode is shown in Figure 5. It has to be clarified that this *I–V* characteristic is not exactly the one of the real tunnel diode within the solar cell, but this *I–V* characteristic can be used to introduce the behavior of the real tunnel diode into the network simulation. The second problem mentioned earlier, that one cannot identify whether the extracted *I–V* curve belongs to the top or to the bottom tunnel diode, still exists. However, measurements of the top and bottom tunnel-diode test structures have shown that the top tunnel diode in use shows the lower J_{Peak}. Therefore, the limiting tunnel diode in the investigated solar cell will be modeled by voltage-dependent current sources as a top tunnel diode. The bottom tunnel diode, in contrast, will be modeled by series resistances with a conductivity of $7\,\mathrm{m\Omega\,cm^2}$. This matches the conductivity measurements of bottom tunnel-diode test structures, showing a value between 5 and $25\,\mathrm{m\Omega\,cm^2}$ while forming a low resistive tunnel junction.

4. VALIDATION OF THE MODEL

4.1. Uniform illumination

The validation of the developed model was carried out with a lattice-matched triple-junction solar cell, the grid layout of which is shown in the left inset of Figure 6(a). This concentrator solar cell with a designated area of about

5 mm^2 was measured under uniform illumination using a triple-source sun simulator and a flash lamp-based system as described in Siefer *et al*. [21]. Note that the calculations of all *I–V* characteristics were performed by the developed network simulation, applying always the same set of input parameters shown in Table I. As only rectangular bus bars can be modeled in the simulation, a slightly different solar cell design was modeled (see right inset of Figure 6a).

A comparison of measured and simulated efficiency for concentration levels between 1 and 1900 suns (1 sun corresponds to 1000 W/m^2) is shown in Figure 6(a). It is assumed that the photocurrent increases linearly with the concentration factor *C*. The simulated data reproduces the increase of efficiency between $C = 1$–500 when the tunnel diode operates as a low resistive contact as well as between high concentrations above $C = 650$–1900 when the tunnel diode operates as a high resistive contact. The

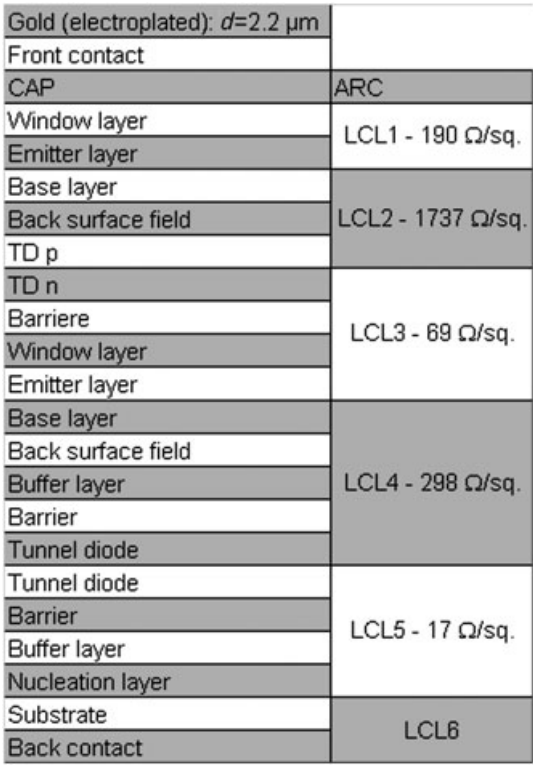

Figure 3. Layer structure of investigated solar cell and the cell participation in respect to lateral current conduction (LCL, lateral conduction layer).

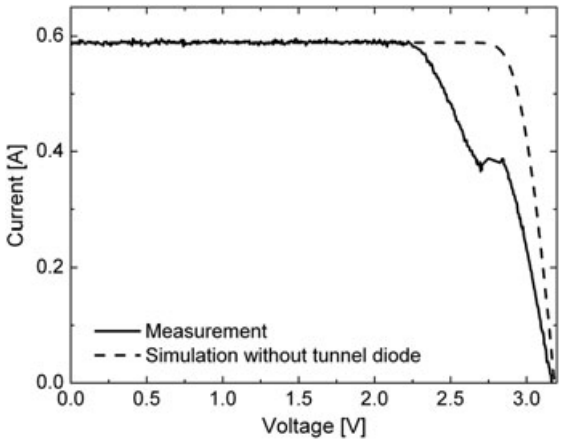

Figure 4. *I–V* characteristic of a lattice-matched triple-junction solar cell measured at 847 suns compared to *I–V* curve calculated without tunnel-diode effects.

Table I. Experimentally obtained material parameters of the investigated triple-junction concentrator solar cell.

Subcell	Parameter	Value	Comment
Top	ρ_M [Ωcm]	2.0E-06	Resistivity of metallization
Top	W_F [µm]	7	Width of grid lines
Top	h_F [µm]	2.2	Height of metallization
Top	ρ_C [Ωcm^2]	3.0E-06	Resistivity of metal–semiconductor contact
Top	R_1 [Ω/sq.]	190	Lateral conducting layer 1
Top	J_{SC} [mA/cm^2]	14.6	Unshaded short circuit current density
Top	J_{01} [A/cm^2]	4.5E-27	Saturation current density in neutral region
Top	J_{02} [A/cm^2]	3.8E-15	Saturation current density in depletion zone
Top	R_2 [Ω/sq.]	1737	Lateral conducting layer 2
Mid	R_3 [Ω/sq.]	69	Lateral conducting layer 3
Mid	J_{SC} [mA/cm^2]	14.9	Unshaded short circuit current density
Mid	J_{01} [A/cm^2]	4.0E-20	Saturation current density in neutral region
Mid	J_{02} [A/cm^2]	2.0E-11	Saturation current density in depletion zone
Mid	R_4 [Ω/sq.]	298	Lateral conducting layer 4
Bot	R_5 [Ω/sq.]	17	Lateral conducting layer 5
Bot	J_{SC} [mA/cm^2]	20.8	Unshaded short circuit current density
Bot	J_{01} [A/cm^2]	1.0E-05	Saturation current density in neutral region
Bot	J_{02} [A/cm^2]	1.0E-04	Saturation current density in depletion zone
All	$\rho_B \cdot d_B$ [Ωcm^2]	9.0E-05	Cumulated resistivity of solar cell layers for vertical current flow
Bot	ρ_{RC} [Ωcm^2]	3.0E-05	Resistivity of back contact

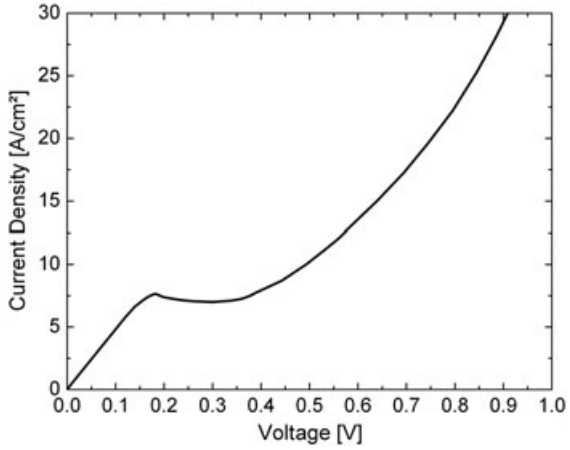

Figure 5. *J–V* characteristic of the current-dependent voltage source to model a tunnel diode.

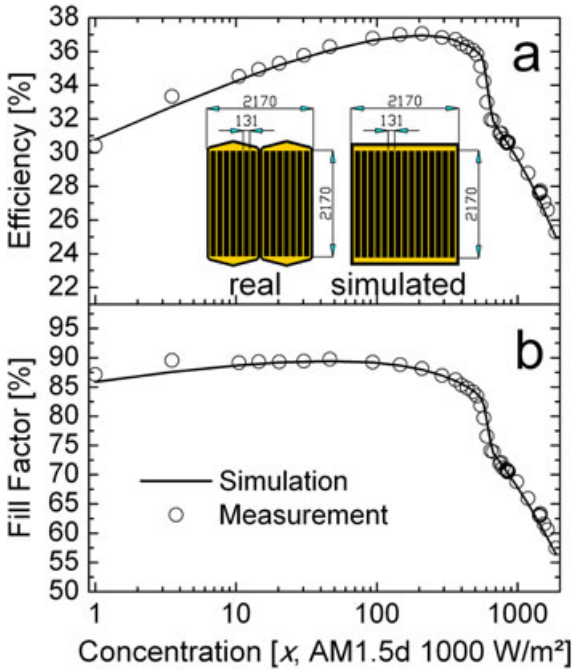

Figure 6. Measured and simulated correlation between efficiency and concentration (a) and fill factor and concentration (b). The simulated data fits the increase in efficiency whereas the tunnel diode operates in the low resistive tunnel mode, as well as the rapid drop caused by the tunnel diode switching to the high resistive thermal diffusion mode. The simulation of the fill factor shows a similar good match with the measurements. In the inset of graph, the real and simulated solar cells are shown. The dimensions are given in μm.

simulation also reproduces the rapid drop between $C = 500$–650, which is caused by the tunnel diode switching to the high resistive thermal diffusion mode. The simulation of the fill factor achieves a similarly good match with the experimentally obtained data (Figure 6b).

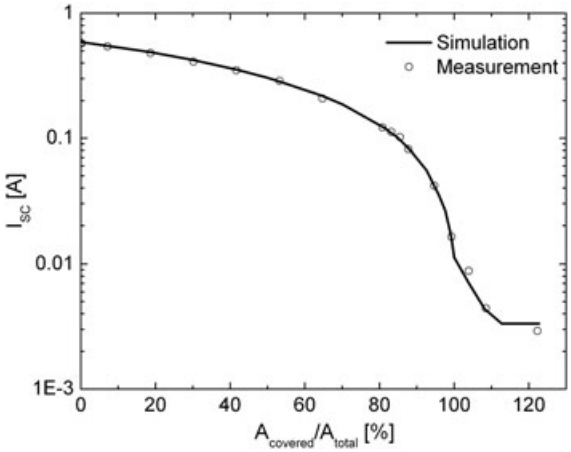

Figure 7. Simulated and measured short circuit current I_{SC} versus the covered part of the area of the solar cell. The partially covered solar cell including the simulated illumination profile is shown in the inset. The good agreement with the measurement data justifies the chosen illumination profile within the simulation.

4.2. Non-uniform illumination

The same triple-junction solar cell and experimental setup as described in Section 4.1 was then used to prove the simulation's capability to calculate the *I–V* characteristics under non-uniform illumination. The illumination profiles were realized by shading the cell with a non-transparent cover. As illustrated in the inset of Figure 7, the edge of the cover was always parallel to the grid lines and was shifted stepwise over the cell. Thus, a digital illumination profile is expected while measuring *I–V* curves at the same intensity of about 850 kW/m^2. However, the measurement of the *I–V* curve taken from the completely covered solar cell revealed that still an intensity of scattered light of around 5 kW/m^2 is available under the cover. This stray light is due to reflection within the measurement equipment. Figure 7 shows the measured short circuit current I_{SC} versus different relations of shadowed area $A_{covered}$ to total area A_{total} of the solar cell. The measured I_{SC} reveals differences to what can be expected from a perfect digital illumination. In consequence, the illumination profile used for the simulation was adjusted until a good match between the calculated and measured data presented in Figure 7 was achieved. The derived illumination profile is sketched in the inlay of Figure 7. It starts with an intensity equivalent to 847 suns upon the uncovered area. At the edge of the cover, the intensity of the illumination profile is 137 suns, dropping linearly to 5 suns after almost 335 μm. The linear drop in the intensity profile under the cover is necessary because the cover is positioned about 500 μm above the solar cell and the incident light of the flash is not perfectly parallel.

The resulting *I–V* curves of the partially covered solar cell are presented in Figure 8. The reduction of the short circuit current is due to the increased shading of the solar cell through the coverage. The comparisons of simulated

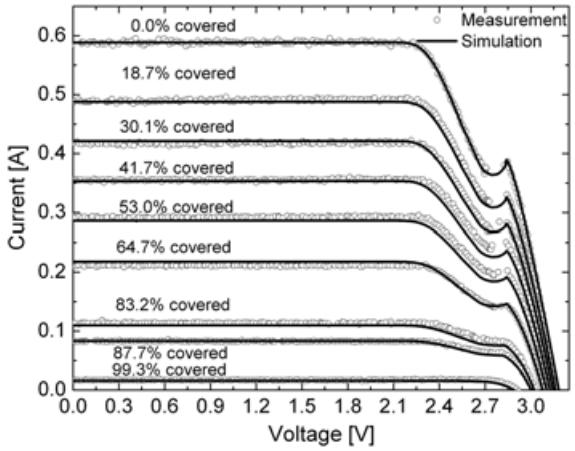

Figure 8. Measured and simulated *I–V* curves of the partially covered triple-junction solar cell. For zero coverage, the illumination intensity was 847 W/m^2. The simulation shows a satisfying agreement with the measurement.

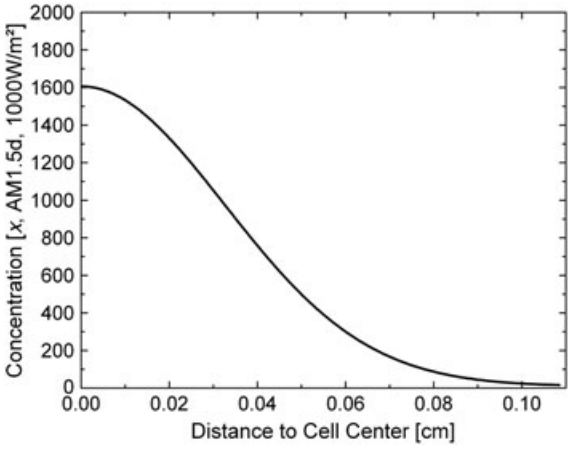

Figure 9. A Gaussian illumination profile is displayed as concentration factor versus distance to cell center. This Gaussian illumination profile, which is similar to realistic profiles in concentrator modules, is applied to model the performance of a triple-junction solar cell.

and measured *I–V* curves show a satisfying agreement. The simulation reproduces also the effects of the tunnel diode that are seen in the measured *I–V* curves. Because of the fact that the simulation has a satisfying agreement with the experimentally derived data, as shown in Figure 8, it can be concluded that the developed network simulation is able to model a triple-junction solar cell including the tunnel-diode transition under non-uniform illumination.

5. RESULTS AND DISCUSSION

Braun *et al*. suggest in their work [13] that a lateral spreading of current exists if a tunnel diode is locally irradiated. In a simulation study, Espinet *et al*. [12] found that a lateral current spreading from high illumination intensity to low-intensity regions can increase the maximum current of the solar cell transported by the tunnel diode before the tunnel diode switches to the thermal diffusion transport mode. Fresnel lenses in concentrator photovoltaic systems nearly apply a Gaussian illumination profile on the solar cell as exemplarily shown in Figure 9. Therefore, the influence of lateral current spreading from high-intensity to low-intensity area might be important in real concentrator systems. As an application of the validated network, the intensity profile shown in Figure 9 is taken and applied to the model of the triple-junction solar cell described in the previous sections. The focus of this profile with a concentration factor of about 1600 suns is assumed to be in the center of the solar cell. This illumination profile has an average concentration of $C = 220$ over the total solar cell area. As described previously, the tunnel diode used for simulation switches to the thermal diffusion mode after $C = 500$. Therefore, the tunnel diode should be able to transport the total amount of current without switching to thermal diffusion. Figure 10 shows calculated *I–V* curves. First, the *I–V* curve of the cell was

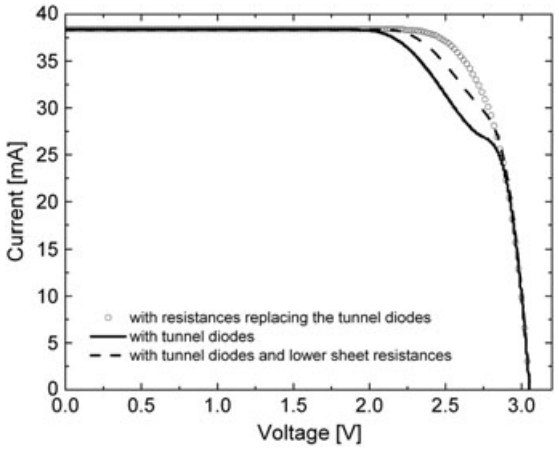

Figure 10. Calculated *I–V* curves of a triple-junction cell with and without tunnel diode effects. Lower sheet resistances of the lateral conducting layer improve the solar cell's performance. All simulations are performed using the Gaussian illumination profile shown in Figure 9.

calculated without any tunnel diode by replacing the tunnel diode by a low resistance. Second, the tunnel diode was implemented in the simulation. The simulation reveals that the lateral current spreading is not enough to drop the current densities under the maximum current density J_{Peak} of the tunnel diode. As a third simulation, the lateral sheet resistance above and below the top tunnel diode (LCL2 and LCL3 in Figure 3) were decreased. The performance of the solar cell rose with this method because of an increase in the lateral current spreading.

In the next step, we used the simulation to investigate the influence of the resistivity of the lateral conduction layers. Starting with the measured sheet resistance of LCL2 of 1737 Ω/sq. and LCL3 of 69 Ω/sq., the maximum

power point of the triple-junction solar cell when a Gaussian illumination profile is applied was calculated. Next, r_{LCL2} and r_{LCL3} are decreased until the resulting maximum power output matches the P_{MPP} calculated without tunnel-diode effects (see Figure 10 dotted line). Figure 11 shows how strong r_{LCL2} and r_{LCL3} have to be decreased in order to increase the lateral current spreading until the current is transported by the tunnel diode without transport in the thermal diffusion mode. For example, when r_{LCL2} is reduced to 1737·0.01 Ω/sq., r_{LCL3} has to be halved. If either r_{LCL2} or r_{LCL3} is kept constant at 1737 Ω/sq. and 69 Ω/sq., respectively, there is no way to prevent the tunnel diode from switching to thermal diffusion transport mode by an improved lateral conduction of the other layer. r_{LCL2} has do be reduced at least to about 1737·0.25 Ω/sq. combined with an r_{LCL3} of 69·0.01 Ω/sq., or alternatively, r_{LCL3} has to be reduced to 69·0.7 Ω/sq. combined with an r_{LCL2} of 1737/300 Ω/sq.

One possibility to realize lower sheet resistances is to introduce additional layers above and below the tunnel diode. Yet, depending on the materials used, additional layers above the middle cell might lead to strong absorption losses of photons, which could otherwise be used by the middle cell for current generation. To keep the absorption in the additional layers low, high band-gap materials need to be used, which should also be as thin and lowly doped as possible. However, these three characteristics are contrary to the low sheet resistance needed for the lateral current spreading, so a compromise needs to be found. As a realistic material option for the lateral conducting layers, $Al_{x-1}Ga_xAs$ was studied. The advantage of AlGaAs is that it can be introduced in lattice-matched triple-junction solar cells with the same lattice constant.

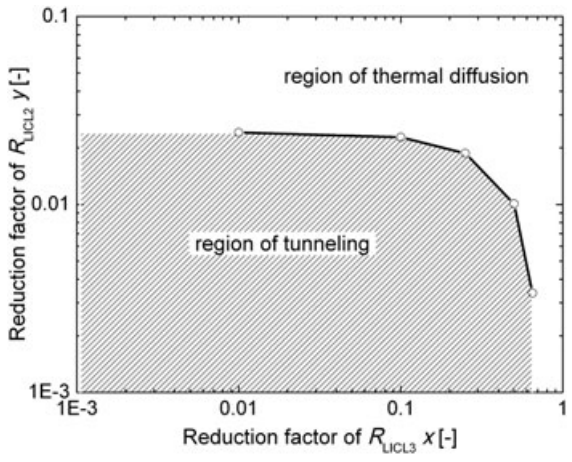

Figure 11. The figure shows by which factor *y*, the resistance of the lateral conduction layer above the tunnel diode, has to be decreased for a distinct reduction of the lateral conduction layer resistance below the tunnel diode by the factor *x*. Every adaption of the lateral resistances by a pair of *x* and *y* prevents the tunnel diodes from switching to the thermal diffusion transport mode under the applied Gaussian illumination profile shown in Figure 9.

Furthermore, the band gap of an AlGaAs layer can be varied between 1.4 and 2.1 eV. Figure 12 shows the calculated minimum thicknesses of these layers in dependence of different mole fractions *x* and doping concentrations of $1{\cdot}10^{18}$, $1{\cdot}10^{19}$, and $1{\cdot}10^{20}\,cm^{-3}$. Note that the sheet resistances that have to be achieved are $r_{LCL2} = 1737{\cdot}0.02$ Ω/sq. and $r_{LCL3} = 69{\cdot}0.25$ Ω/sq. as discussed in Figure 11. The mobilities, depending on mole fraction *x*, are calculated with the model by Sotoodeh *et al.* [20].

The results presented in Figure 12 show that if a thin layer is demanded, a low value for the band gap and a very high doping concentration of above $1{\cdot}10^{20}\,cm^{-3}$ are necessary. The thinnest feasible layer with a doping concentration of $1{\cdot}10^{20}\,cm^{-3}$ consists of GaAs with a thickness of about 30 nm for the n-doped layer and 300 nm for the p-doped layer. However, GaAs would absorb photons, which are of use for the middle cell. Moreover, the free carrier absorption increases strongly for doping concentrations above $n = 6.7{\cdot}10^{18}\,cm^{-3}$ and $p = 5{\cdot}10^{18}\,cm^{-3}$ [22]. $Al_xGa_{1-x}As$ would be a better choice, because it becomes an indirect gap semiconductor for mole fractions higher than 0.55 [23]. For the p-doped $Al_xGa_{1-x}As$ layers, the minimal thickness at a mole fraction of $x = 1.0$ is 0.9 µm with $p = 1{\cdot}10^{20}\,cm^{-3}$ (4.75 µm at $p = 1{\cdot}10^{19}\,cm^{-3}$, 24.24 µm at $p = 1{\cdot}10^{18}\,cm^{-3}$) achieving a band gap of about 2.17 eV [23]. For n-doped layers, the minimal thickness at a mole fraction of $x = 0.55$ is about 1.9 µm with $n = 1{\cdot}10^{20}\,cm^{-3}$ (8.6 µm at $n = 1{\cdot}10^{19}\,cm^{-3}$, 26.3 µm at $n = 1{\cdot}10^{18}\,cm^{-3}$). Therefore, it can be summarized that either a high doping concentration above $1{\cdot}10^{20}\,cm^{-3}$ is needed or layer thicknesses greater than 10 µm are necessary to increase the lateral current spreading sufficiently. Furthermore, it is important to mention that two layers have to be introduced in the solar cell in any case: one p-doped layer above the tunnel diode and one n-doped layer below the tunnel diode.

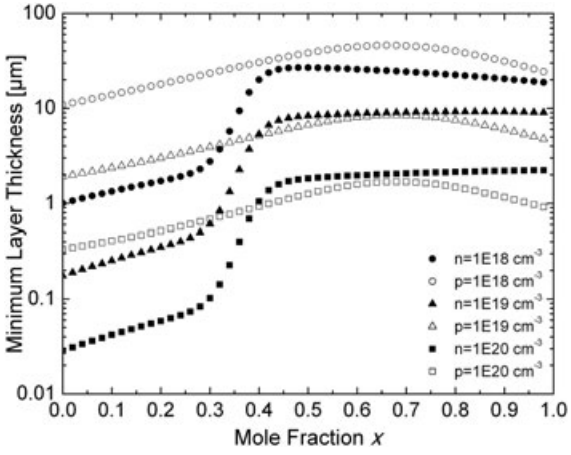

Figure 12. Minimum thickness of $Al_xGa_{1-x}As$ lateral conduction layers as a function of the mole fraction *x*, which is necessary to increase the lateral current spreading in order to prevent the tunnel diode from switching to the thermal diffusion transport mode. Filled symbols represent p-doped layers and unfilled symbols n-doped layers.

6. CONCLUSIONS

A model based on distributed network simulation for modeling triple-junction solar cells, including the tunnel-diode transition, has been presented. The tunnel-diode effects were integrated into the network simulation by voltage-dependent current sources. The model was verified with experimental data derived from a lattice-matched triple-junction concentrator solar cell having a tunnel diode switching to the thermal diffusion mode at homogenous illumination intensities of about 500 suns. The validation of the network model was performed under homogeneous illumination between 1 and 1900 suns and also with a non-uniform quasi-digital illumination of the solar cell. The comparison of simulated and measured data showed a good agreement. Assuming a Gaussian illumination profile with an average concentration of $C = 220$, the network simulation was used to demonstrate that in this case, the lateral current flow from high to low illumination intensity regions cannot prevent the tunnel diode from switching into the thermal diffusion transport mode. In addition, in this work, a study was performed to evaluate an increase of lateral current spreading through a reduction of lateral sheet resistances. It is demonstrated that at least one additional layer above and one layer below the tunnel diode have to be introduced into a lattice-matched triple-junction solar cell to increase the current spreading enough to transport all current exclusively by tunneling. As a realization of low resistive lateral conducting layers for the improvement of a solar cell's tunneling capability, $Al_xGa_{1-x}As$ was evaluated. It can be concluded that $Al_xGa_{1-x}As$ layer thicknesses larger than 10 µm are needed if the doping concentration is below $1{\cdot}10^{18}\,cm^{-3}$. For doping concentrations above $1{\cdot}10^{20}\,cm^{-3}$, the minimum layer thickness for the n-GaAs layers would be 30 nm and for the p-GaAs layer would be 300 nm. For reduction of photon absorption, $Al_xGa_{x-1}As$ with $x > 0.55$ might be used because of its indirect band gap. However, even for an n-$Al_{0.55}Ga_{0.45}As$ and $n = 1{\cdot}10^{20}\,cm^{-3}$, a layer thickness of 1.9 µm and 0.9 µm for p-AlAs are needed, and the free carrier absorption losses must be considered.

ACKNOWLEDGEMENTS

The authors would like to thank all the colleagues of the "III–V Epitaxy and Solar Cell" group for their contributions to this paper. This work has been partly supported by the Federal Ministry for the Environment, Nature Conservation and Nuclear Safety (BMU) under the KoMGen project, contract number 0327567A. The authors are responsible for the content of this paper.

REFERENCES

1. Green MA, Emery K, Hishikawa Y, Warta W. Solar cell efficiency tables (version 36). *Progress in Photovoltaics: Research and Applications* 2010; **18**(5): 346.
2. Guter W, Bett AW. *I–V* Characterization of Tunnel Diodes and Multijunction Solar Cells. *IEEE Transactions on Electron Devices* 2006; **53**(9): 2216.
3. Blume W. Computer circuit simulation. *Byte* 1986; **11**(7): 165.
4. Steiner M, Philipps SP, Hermle M, Bett AW, Dimroth F. Validated front contact grid simulation for GaAs solar cells under concentrated sunlight. *Progress in Photovoltaics: Research and Applications* 2010; **19**(**1**): 73. DOI: 10.1002/pip.989
5. Galiana B, Algora C, Rey-Stolle I. Explanation for the dark I–V curve of III–V concentrator solar cells. *Progress in Photovoltaics: Research and Applications* 2008; **16**(4): 331.
6. Nishioka K, Takamoto T, Nakajima W, *et al*. Analysis of triple-junction solar cell under concentration by SPICE. *Proceedings of the 3rd World Conference on Photovoltaic Energy Conversion*, 2003; 869.
7. Garcia I, Algora C, Rey-Stolle I, Galiana B. Study of non-uniform light profiles on high concentration III–V solar cells using quasi-3D distributed models. *Proceedings of the Photovoltaic Specialists Conference*, 2008; 1.
8. Philipps SP, Hermle M, Létay G, Dimroth F, BM George, Bett AW. Calibrated numerical model of a GaInP-GaAs dual-junction solar cell. *Physica Status Solidi RRL: Rapid Research Letters* 2008; **2**(4): 166–68.
9. Baudrit M, Algora C. Modeling of GaInP/GaAs dual-junction solar cells including tunnel junction. *Proceedings of the 33rd IEEE Photovoltaic Specialists Conference*, 2008; 576.
10. Li ZQ, Xiao YG, Li ZMS. Modeling of multi-junction solar cells by Crosslight APSYS. *Proceedings of SPIE—the International Society for Optical Engineering*, 2006; 633909.
11. Hermle M, Létay G, Philipps SP, Bett AW. Numerical simulation of tunnel diodes for multi-junction solar cells. *Progress in Photovoltaics: Research and Applications* 2008; **16**(5): 409.
12. Espinet P, Garcia I, Rey-Stolle I, Algora C, Baudrit M. Distributed simulation of real tunnel junction effects in multi-junction solar cells. *Proceedings of the 6th International Conference on Concentrating Photovoltaic Systems*, 2010; 24.
13. Braun A, Hirsch B, Katz EA, Gordon JM, Guter W, Bett AW. Localized irradiation effects on tunnel diode transitions in multi-junction concentrator solar cells. *Solar Energy Materials and Solar Cells* 2009; **93**(9): 1692.
14. Nielsen LD. Distributed series resistance effects in solar cells. *IEEE Transactions on Electron Devices* 1982; **29**(5): 821.

15. Galiana B, Rey-Stolle I, Algora C, Baudrit M, Garcia I. 3D distributed model for concentrator solar cells. *Proceedings of the 19th European Photovoltaic Solar Energy Conference*, 2004; 348.
16. LTSpice. Switcher CAD III/LT Spice, 2007. http://www.linear.com/software [accessed on 15/07/2010]
17. Baur C, Bett AW. Modelling of III–V multi-junction cells based on spectrometric characterisation. *Proceedings of the 20th European Photovoltaic Solar Energy Conference*, 2005; 183.
18. Bowden S, Yelundur V, Rohatgi A. Implied-V_{oc} and Suns-V_{oc} measurements in multicrystalline solar cells. *Proceedings of the 29th IEEE Photovoltaic Specialists Conference*, 2002; 371.
19. Reeves GK, Harrison HB. Obtaining the specific contact resistance from transmission line model measurements. *IEEE Electron Device Letters* 1982; **3**(5): 111.
20. Sotoodeh M, Khalid AH, Rezazadeh AA. Empirical low-field mobility model for III–V compounds applicable in device simulation codes. *Journal of Applied Physics* 2000; **87**(6): 2890.
21. Siefer G, Baur C, Meusel M, Dimroth F, Bett AW, Warta W. Influence of the simulator spectrum on the calibration of multi-junction solar cells under concentration. *Proceedings of the 29th IEEE Photovoltaics Specialists Conference*, 2002; 836.
22. Levinshtein M, Rumyantsev S, Shur M (eds). Si, Ge, C (Diamond), GaAs, GaP, GaSb, InAs, InP, InSb. Handbook Series on Semiconductor Parameters, World Scientific Publishing Co. Pte. Ltd., Singapore, 1996.
23. Levinshtein M, Rumyantsev S, Shur M. Ternary and Quaternary III–V Compounds. World Scientific Publishing Co. Pte. Ltd.: Singapore, 1999.

DOI: 10.1002/pip